Available online at www.sciencedirect.com
SCIENCE DIRECT®
Journal of Solid State Chemistry 177 (2004) 4346–4350
JOURNAL OF SOLID STATE CHEMISTRY
http://elsevier.com/locate/jssc

# Hydrothermal synthesis, crystal structure, and magnetic property of a three-dimensional inorganic–organic hybrid material: $Mn(H_2O)[HO_3PCH_2NH(CH_2CO_2)_2]$

Yong Fan, Guanghua Li, Zhan Shi, Dong Zhang, Jianing Xu, Tianyou Song,* and Shouhua Feng*

*State Key Laboratory of Inorganic Synthesis and Preparative Chemistry, College of Chemistry, Jilin University, Qianwei Road 10, Changchun City, Jilin Province 130012, PR China*

Received 26 March 2004; received in revised form 10 May 2004; accepted 14 May 2004

**Abstract**

A novel three-dimensional inorganic–organic hybrid compound, $Mn(H_2O)[HO_3PCH_2NH(CH_2CO_2)_2]$ from a hydrothermal reaction of Mn (II) ion with *N*-(phosphonomethyl)iminodiacetic acid ($H_4PMIDA$) was reported. The compound crystallizes in the monoclinic $P2_1/n$ with cell dimensions of $a = 5.215(5)$ Å, $b = 14.111(15)$ Å, $c = 12.727(12)$ Å, $\beta = 93.646(16)°$, $V = 934.6(16)$ Å$^3$ and $Z = 4$. In this structure each Mn atom is six-coordinated with the carboxylic groups and phosphonic groups to form layers along the *bc* plane. These layers are further connected with the organic moieties of $H_2PMIDA$, resulting in a complicated three-dimensional network structure. Thermogravimetric analysis, IR spectrum and magnetic susceptibility of this compound are given.


*Keywords:* Hydrothermal synthesis; Metal phosphonate; Structure; Property; Magnetic susceptibility

## 1. Introduction

In recent years, metal phosphonate chemistry was extensively studied partially due to the potential applications of metal phosphonates in catalysis, molecular recognition, ion exchange, non-linear optics and sensors [1–7]. Great efforts have been devoted to the syntheses of novel inorganic–organic hybrid materials based on metal phosphonates, which exhibit a variety of structures such as one-dimensional (1D) chain, two-dimensional (2D) layer, and three-dimensional (3D) network [8–10]. Synthesis of the metal phosphonate compounds containing functional groups of carboxylate, amine and crown ether [11–14], and even metal amino-carboxylate-phosphonates were less investigated [7–13]. In the point of view of structural construction of inorganic–organic hybrid compounds, phosphonic acids with additional carboxylic functional groups are useful ligands, because they together provide coordination sites which may increase the solubility of the metal phosphonates in water and improve the crystallinity of their metal complexes [10]. Compounds with open framework structures based on *N*-(phosphonomethyl)iminodiacetic acid ($H_4PMIDA$), which can adopt various kinds of coordination modes under different reaction conditions were found to form metal phosphonates with 1D, 2D and 3D structures [15–21]. In this paper, we report the synthesis, crystal structure, thermal and magnetic properties of a novel 3D manganese coordination compound containing $H_4PMIDA$ as ligand, $Mn(H_2O)[HO_3PCH_2NH(CH_2CO_2)_2]$ **1**.

## 2. Experimental

### 2.1. Synthesis and characterization

In a typical synthesis, 0.199 g of $MnCl_2 \cdot 4H_2O$ was dispersed and dissolved in 10 mL of water, followed by

*Corresponding author. Fax: +86-431-5168624.
*E-mail address:* fanyong1977@hotmail.com (S. Feng).

0022-4596/$ - see front matter © 2004 Elsevier Inc. All rights reserved.
doi:10.1016/j.jssc.2004.05.021

addition of 0.234 g of $H_4$PMIDA on stirring vigorously, to form a solution. 1.2 mL of tatramethylammonium hydroxide solution (15%, TMAOH) was added to this solution with continue stirring until a homogeneous reaction mixture was formed. The final mixture with a molar ratio of 1 $MnCl_2 \cdot 4H_2O$:1 $H_4$PMIDA:4 TMAOH was crystallized in a 23 mL PTFE-lined acid digestion bomb at 150°C for 5 days. The resultant product of pink needles was filtered and washed thoroughly with distilled water. The yield of product was 75% in weight based on Manganese.

The elemental analysis was conducted on a Perkin-Elmer 2400LC II elemental analyzer. Inductively coupled plasma (ICP) analysis was performed on a Perkin-Elmer Optima 3300DV ICP instrument. X-ray powder diffraction (XRD) data were collected on a Siemens D5005 diffractometer with Cu$K\alpha$ radiation ($\lambda = 1.5418$ Å). The step size was 0.02°, and the count time was 4 s. The infrared (IR) spectrum was recorded within the 400–4000 $cm^{-1}$ region on a Nicolet Impact 410 FTIR spectrometer using KBr pellets. A Perkin-Elmer DTA 1700 differential thermal analyzer was used to obtain the differential thermal analysis (DTA) and a Perkin-Elmer TGA 7 thermogravimetric analyzer to obtain thermogravimetric analysis (TGA) curves in an atmospheric environment with a heating rate of 10°C $min^{-1}$. Magnetic susceptibility data were collected on the basis of a 0.0475 g sample over the temperature range 2.4–300 K at a magnetic field of 5 kG on a Quantum Design MPMS-7 SQUID magnetometer.

### 2.2. Determination of the crystal structures

A suitable pink single crystal with dimensions $0.25 \times 0.25 \times 0.20\,mm^3$ was glued to a thin glass fiber and mounted on a Siemens Smart CCD diffractometer equipped with a normal-focus, 2.4-kW sealed-tube X-ray source (graphite-monochromatic Mo$K\alpha$ radiation ($\lambda = 0.71073$ Å). Intensity data were collected at a temperature of $298 \pm 2$ K. Date processing was accomplished with the SAINT processing program [22]. The total number of measured reflections and observed unique reflections were 4979 and 2290, respectively. Intensity data of 2290 independent reflections ($-6 \leqslant h \leqslant 6$, $-18 \leqslant k \leqslant 13$, $-16 \leqslant l \leqslant 13$) were collected in the $\omega$-scan mode. An empirical absorption correction was applied using the SADABS program with $T_{max} = 0.2774$ and $T_{min} = 0.2388$). The structure was solved in the space group $P2_1/n$ by direct methods and refined on $F^2$ by full-matrix least squares using SHELXTL97 [23]. The phosphorus and manganese atoms were located first. Carbon, nitrogen, and oxygen were then found in the difference Fourier map. The hydrogen atoms that are bonded to carbon and nitrogen atoms were placed geometrically. All non-hydrogen atoms were refined with anisotropic thermal parameters. A summary of the crystallographic data is presented in Table 1. Final atomic positional and thermal parameters for **1** are given in Table 2, and selected bond distance and bond angle data are summarized in Table 3.

Table 1
Crystallographic data for **1**

| | |
|---|---|
| Empirical formula | $C_5H_{10}NO_8PMn$ |
| Formula weight | 298.05 |
| Temperature | 298(2) K |
| Crystal system | Monoclinic |
| Space group | $P2_1/n$ |
| $a$ | 5.215(5) Å |
| $b$ | 14.111(15) Å |
| $c$ | 12.727(12) Å |
| $\beta$ | 93.646(16)° |
| $V$ | 934.6(16) $Å^3$ |
| $Z$ | 4 |
| Calculated density | 2.118 $Mg/m^3$ |
| Absorption coefficient | 1.615 $mm^{-1}$ |
| $\lambda$(Mo$K\alpha$) | 0.71073 Å |
| Crystal size | $0.25 \times 0.25 \times 0.20\,mm^3$ |
| Reflections collected/unique | 4979/2290 [$R_{int} = 0.0901$] |
| $F$(0 0 0) | 604 |
| Data/restraints/parameters | 2290/0/153 |
| Goodness-of-fit on $F^2$ | 0.844 |
| Final $R$ indices [$I > 2\sigma(I)$]* | $R_1 = 0.0550$; w$R_2 = 0.0876$ |
| $R$ indices (all data) | $R_1 = 0.1175$; w$R_2 = 0.1003$ |

*Note*:
$R_1 = \Sigma||F_o| - |F_c||/\Sigma|F_o|$; w$R_2 = \{\Sigma[w(F_o^2 - F_c^2)^2]/\Sigma[w(F_o^2)]^2\}^{1/2}$.

Table 2
Atomic coordinates ($\times 10^4$) and equivalent isotropic displacement parameters ($Å^2 \times 10^3$) for **1**

| | $x$ | $y$ | $z$ | $U_{eq}$ |
|---|---|---|---|---|
| Mn(1) | 3533(2) | 7670(1) | 5223(1) | 18(1) |
| N(1) | 3932(7) | 5143(3) | 2368(3) | 16(1) |
| P(1) | 4514(3) | 3184(1) | 2319(1) | 18(1) |
| O(1) | 2902(6) | 2935(2) | 1342(2) | 22(1) |
| O(2) | 4778(6) | 2454(2) | 3184(2) | 23(1) |
| O(3) | 7226(6) | 3538(3) | 2000(2) | 25(1) |
| O(4) | 6128(6) | 6543(2) | 4644(2) | 24(1) |
| O(5) | 7880(7) | 5355(3) | 3785(3) | 32(1) |
| O(6) | 5842(7) | 6158(3) | 766(3) | 27(1) |
| O(7) | 1865(7) | 6388(2) | −26(2) | 24(1) |
| O(8) | 920(8) | 6556(3) | 5532(3) | 30(1) |
| C(1) | 3208(10) | 4238(4) | 2910(3) | 19(1) |
| C(2) | 3887(10) | 5969(4) | 3101(4) | 23(1) |
| C(3) | 6160(10) | 5939(4) | 3903(4) | 20(1) |
| C(4) | 2268(9) | 5318(4) | 1384(3) | 19(1) |
| C(5) | 3466(10) | 6026(4) | 659(4) | 19(1) |

*Note*: $U$(eq) is defined as one third of the trace of the orthogonalized $U_{ij}$ tensor.

## 3. Results and discussion

### 3.1. Characterization

ICP analysis for the product gave the contents of Mn 18.36 wt% (calcd 18.43 wt%) and P 10.44% (calcd

Table 3
Selected bond lengths (Å) and angles (°) for **1**

| | | | |
|---|---|---|---|
| Mn(1)–O(1)#1 | 2.116(4) | Mn(1)–O(8) | 2.133(4) |
| Mn(1)–O(2)#2 | 2.166(4) | P(1)–O(1) | 1.498(3) |
| Mn(1)–O(4) | 2.242(4) | P(1)–O(2) | 1.507(4) |
| Mn(1)–O(6)#4 | 2.303(4) | P(1)–O(3) | 1.577(4) |
| Mn(1)–O(7)#3 | 2.226(4) | P(1)–C(1) | 1.818(5) |
| | | | |
| O(1)#1–Mn(1)–O(2)#2 | 173.70(13) | O(8)–Mn(1)–O(2)#2 | 89.66(14) |
| O(1)#1–Mn(1)–O(4) | 90.05(13) | O(8)–Mn(1)–O(4) | 86.80(17) |
| O(1)#1–Mn(1)–O(6)#4 | 88.25(13) | O(8)–Mn(1)–O(6)#4 | 93.73(17) |
| O(1)#1–Mn(1)–O(7)#3 | 89.58(13) | O(8)–Mn(1)–O(7)#3 | 168.43(15) |
| O(2)#2–Mn(1)–O(6)#4 | 89.81(13) | O(1)–P(1)–O(2) | 117.8(2) |
| O(2)#2–Mn(1)–O(7)#3 | 84.68(13) | O(1)–P(1)–O(3) | 108.99(19) |
| O(2)#2–Mn(1)–O(4) | 91.85(13) | O(2)–P(1)–O(3) | 111.24(19) |
| O(4)–Mn(1)–O(6)#4 | 178.26(12) | O(1)–P(1)–C(1) | 109.3(2) |
| O(7)#3–Mn(1)–O(4) | 83.31(15) | O(2)–P(1)–C(1) | 106.0(2) |
| O(7)#3–Mn(1)–O(6)#4 | 96.33(15) | O(3)–P(1)–C(1) | 102.4(2) |

*Note*: Symmetry transformations used to generate equivalent atoms: $\#1 - x + 1/2, y + 1/2, -z + 1/2; \#2 - x + 1, -y + 1, -z + 1; \#3 x + 1/2, -y + 3/2, z + 1/2; \#4 x - 1/2, -y + 3/2, z + 1/2$.

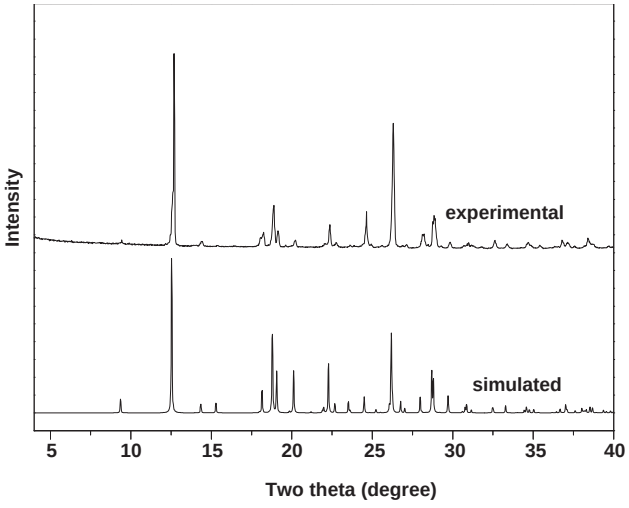


Fig. 1. Experimental and simulated power X-ray diffraction patterns for **1**.

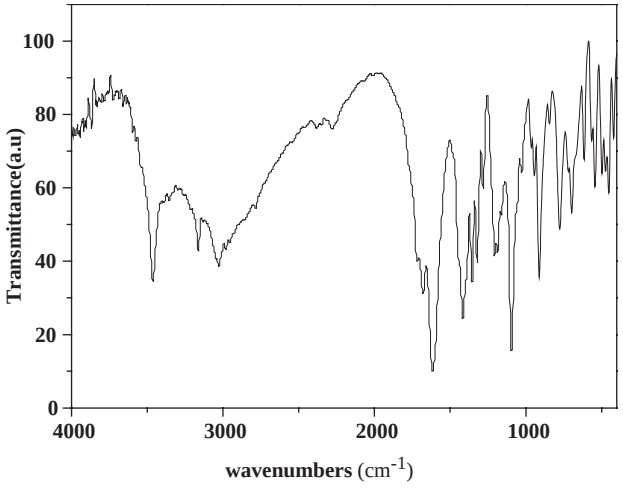


Fig. 2. Infrared spectra of **1**.

10.39 wt%), indicating an Mn:P ratio of 1:1. Elemental analysis showed 20.26, 3.58, and 4.64 wt% of C, H, and N, respectively, in agreement with the experimental values of 20.13, 3.36, and 4.70 wt% of C, H, and N based on the ideal formula given by single-crystal X-ray diffraction analysis.

Powder X-ray diffraction pattern was consistent with the simulated one based on the X-ray diffraction analysis, as shown in Fig. 1. The diffraction peaks on both patterns are corresponded well in positions, indicating the phase purity of the as-synthesized sample.

IR spectrum was recorded between 4000 and 400 $cm^{-1}$ (Fig. 2) The sharp band at 3466 $cm^{-1}$ is attributed to O–H asymmetric stretching vibrations of the lattice water and PO–H. The band centered at 3351 $cm^{-1}$ is due to N–H stretching. The C–H stretching vibrations are observed as a sharp and weak band at 3157 $cm^{-1}$ and a broad band at 3030 $cm^{-1}$. A weak band centered at 1712 $cm^{-1}$ is due to the bending C=O vibration of the carboxylate. The P–OH stretching vibrations are observed as a sharp band close to 1095 $cm^{-1}$. The remaining vibration bands are those typical of the *N*-(phosphonomethyl)iminodiacetic salts.

Combined TGA–DTA curves for **1** are shown in Fig. 3. The strong endotherm, centered at 299°C, is due to the loss of hydration water molecules and carboxylates. The calculated weight loss for this process is 41.61% and the observed weight loss is 41.81%. The combustion of the organic started at 420°C with an endotherm and then exotherms at 532°C and 613°C, respectively. TGA curve showed a continuous weight loss in this region of temperature. The final thermal decomposition products at 800°C were $Mn_2P_4O_{12}$ with its standard powder diffraction pattern (PDF database No: 36–0210) and MnO (PDF database No: 36–0210).

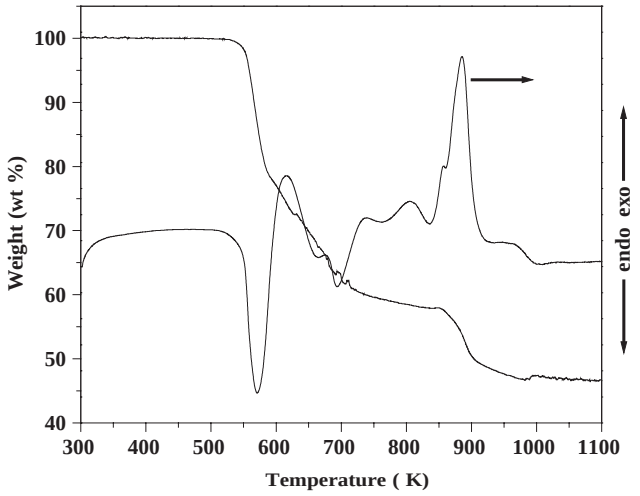


Fig. 3. TGA–DTA curves for **1**.

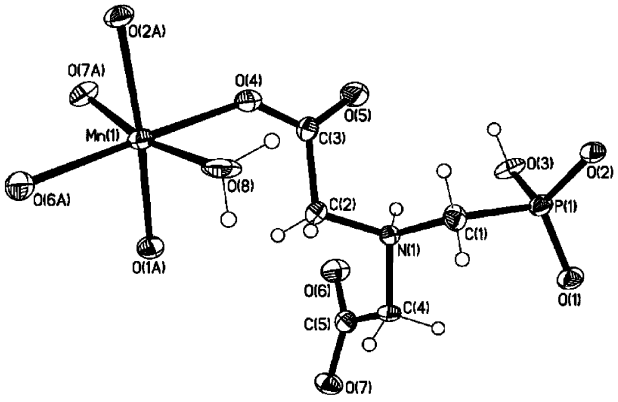


Fig. 4. ORTEP view of the structure of 1 showing the atom-labeling scheme (50% thermal ellipsoids).

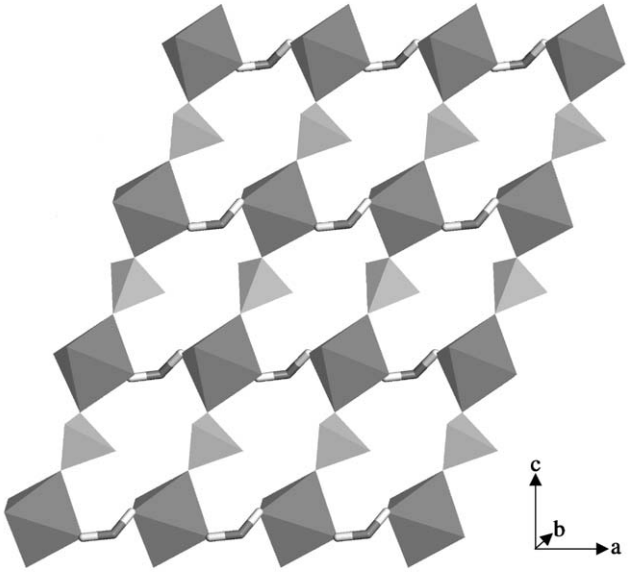


Fig. 5. Carboxylate groups (O6–C5–O7) of the phosphonate, connect the chains generated by $\{MnO_6\}$ octahedron-$\{-PO_3H\}$ tetrahedron into 2D layers along ac plane. $\{-PO_3H\}$ tetrahedral are white and $\{MnO_6\}$ octahedron are gray.

### 3.2. Description of structure

The asymmetric unit of **1,** as shown in Fig. 4, consists of one manganese atom, one water molecule and one $H_2$PMIDA ligand. Mn atom has a distorted octahedral coordination. The basal plane is defined by the three oxygen atoms from three equivalent *N*-(phosphonomethyl) iminodiacetic acid ligands and a water molecule. The bond angles of O–Mn–O are in a range of 83.31(15)–96.33(15)°. The bond lengths of Mn(1)–O(6A), Mn1–O(7A), Mn(1)–O(4) and Mn(1)–O(8) are 2.303(4), 2.226(4), 2.242(4) and 2.133(4) Å, respectively. Two axial sites are provided by O(1A) and O(2A) from two equivalent phosphonate ligands at distances of 2.116(4) Å and 2.166(4) Å, respectively.

The coordination mode of the PMIDA in **1** is different from that in another compound synthesized from PMIDA [21]. In compound of **1**, two carboxylate groups of $H_2$PMIDA ligands have two coordination modes. In the first mode the carboxylate group acts as a monodentate ligand to bind a manganese ion. Another oxygen atom O(5) forms a hydrogen bond with a water molecule with an O(8)···O(5) distance of 2.890 Å. In the second mode it serves as a bidentate ligand to bridge two manganese centers. The phosphonate group bridge with two metal ions using O(1) and O(2) atoms. N(1) is protonated.

The structure of **1** contains chains of $\{MnO_6\}$ and $\{-PO_3H\}$ by alternatively corner-sharing. These chains are linked by carboxylate groups (O6−C5−O7) into 2D layers in the *ac*-plane (Fig. 5). These layers are further connected with the organic moieties of $H_2$PMIDA pillars, resulting in the formation of a complicated 3D network (Fig. 6).

### 3.3. Magnetic susceptibility

The temperature dependence of magnetic susceptibility ranging from 2.4 to 300 K for **1** was measured (Fig. 7). The experimental data were fitted using the Curie-Weiss equation $X_m = C_m/(T-\theta)$, with $C_m = 1.000\,\text{emu}\,\text{K}^{-1}\,\text{mol}^{-1}$ and $\theta = -0.2351$ K. This result indicates there exists a weak antiferromagnetic interaction in the title compound. At 300 K, the calculated effective magnetic moment for per manganese atom, $\mu_{\text{eff}} = 5.75\mu_B$, in a good agreement with the predicted spin-only value of $5.91\mu_B$ for a $d^5$ manganese(II).

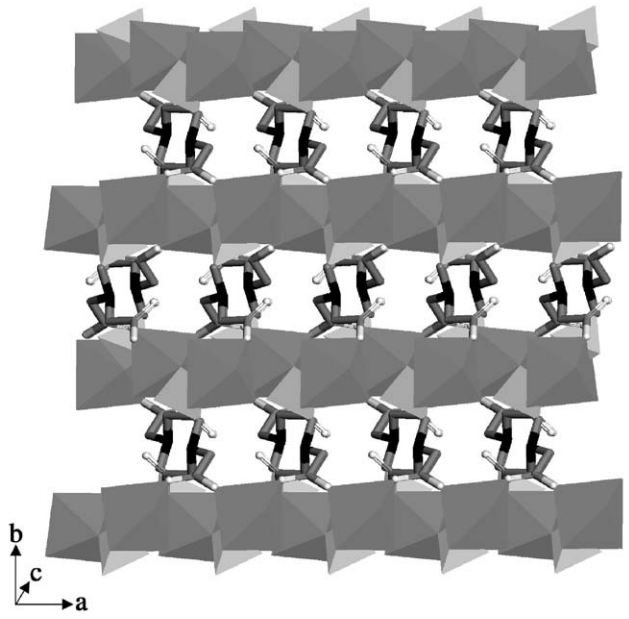


Fig. 6. View of crystal structure of the complex along the *c*-axis. $PO_3H$ tetrahedra are white and $MnO_6$ octahedra are gray.

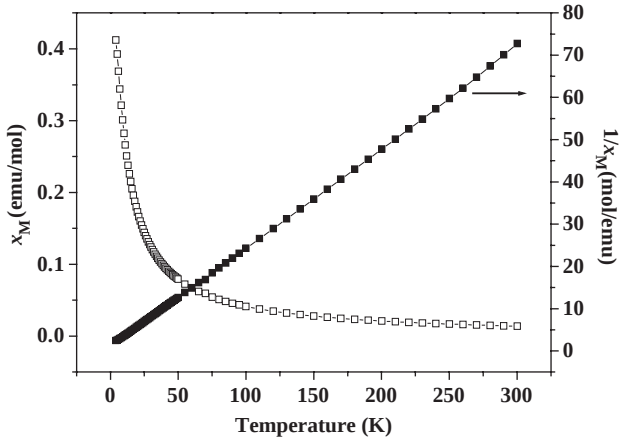


Fig. 7. Thermal evolution of $X_m$ (□) and $1/X_m$ (■) curves of **1**.

## 4. Conclusions

A novel 3D inorganic–organic hybrid compound $Mn(H_2O)[HO_3PCH_2NH(CH_2CO_2)_2]$ has been hydrothermally synthesized from the Mn (II) ion and $H_4$PMIDA and structurally characterized by single crystal X-ray diffraction analysis. The product is pure phase confirmed by powder X-ray diffraction. The structure consists of alternatively connected $\{MnO_6\}$–$\{-PO_3H\}$ chains linked by carboxylates binders and $H_2$PMIDA pillars, forming a novel 3D network This compound is stable below 299°C. The temperature dependence of magnetic susceptibility shows a weak antiferromagnetic interaction in the compound.

## Acknowledgments

We thank the National Natural Science Foundation of China (Grant No. 20071013 and 20301007), the State Basic Research Project of China (Grant G2000077507).

## References

[1] C. Maillet, P. Janvier, M. Pipelier, T. Praveen, Y. Andres, B. Bujoli, Chem. Mater. 13 (2001) 2879.
[2] I.O. Benitez, B. Bujoli, L.J. Camus, C.M. Lee, F. Odobel, D.R. Talham, J. Am. Chem. Soc. 124 (2002) 4363.
[3] V.V. Krishnan, A.G. Dokoutchaev, M.E. Thompson, J. Catal. 196 (2000) 366.
[4] G. Cao, H. Hong, T.E. Mallouk, Acc. Chem. Res. 25 (1992) 420.
[5] B. Zhang, A. Clearfield, J. Am. Chem. Soc. 119 (1997) 2751.
[6] H.E. Katz, G. Scheller, T.M. Putvinski, M.L. Schilling, W.L. Wilson, C.E.D. Chidsey, Science 254 (1991) 1485.
[7] G. Alberti, in: J.M. Lehn (Ed.), Comprehensive Supramolecular Chemistry, Pergamon, Elsevier Science Ltd., Oxford, UK, 1996, p. 7.
[8] E. Stein, A. Clearfield, M.A. Subramanian, Solid State Ionics. 83 (1996) 113.
[9] A. Clearfield, Curr. Opin. Solid State Mater. Sci. 1 (1996) 268.
[10] A. Clearfield, Metal phosphonate chemistry, in: K.D. Karlin (Ed.), Progress in Inorganic Chemistry, Vol. 47, Wiley, New York, 1998, pp. 371–510 (and references therein).
[11] F. Fredoueil, M. Evain, D. Massiot, M. Bujoli-Doeu, B. Bujoli, J. Mater. Chem. 11 (2001) 1106.
[12] M. Riou-Cavellec, M. Sanselme, M. Nogues, J.M. Greneche, G. Ferey, Solid State Sci. 4 (2002) 619.
[13] A. Clearfield, D.M. Poojary, B. Zhang, B. Zhao, A. Derecskei-Kovacs, Chem. Mater. 12 (2000) 2745.
[14] P. Ayyappan, O.R. Evans, B.M. Foxman, K.A. Wheeler, T.H. Warren, W.B. Lin, Inorg. Chem. 40 (2001) 5954.
[15] B. Zhang, D.M. Poojary, A. Clearfield, Inorg. Chem. 37 (1998) 249.
[16] D.M. Poojary, B. Zhang, A. Clearfield, Angew. Chem. Int. Ed. Engl. 33 (1994) 2324.
[17] B. Zhang, D.M. Poojary, A. Clearfield, G.-Z. Peng, Chem. Mater. 8 (1996) 1333.
[18] D.M. Poojary, A. Clearfield, J. Organomet. Chem. 512 (1996) 237.
[19] S.O.H. Gutschke, D.J. Price, A.K. Powell, P.T. Wood, Angew. Chem. Int. Ed. 38 (1999) 1088.
[20] J.-G. Mao, A. Clearfield, Inorg. Chem. 41 (2002) 2319.
[21] J.-G. Mao, Z. Wang, A. Clearfield, Inorg. Chem. 41 (2002) 6106.
[22] Software Packages SMART and SAINT, Siemens Analytical X-ray Instruments, Inc., Madison, WI, 1996.
[23] SHELXTL, version 5.1; Siemens Industrial Automation, Inc, Madison, WI, 1997.